

## Coexistence of reconstructed and unreconstructed structures in the structural transition regime of twisted bilayer graphene

Xiao-Feng Zhou<sup>1</sup>, Yi-Wen Liu<sup>1</sup>, Chen-Yue Hao<sup>1</sup>, Chao Yan<sup>1</sup>, Qi Zheng<sup>1</sup>, Ya-Ning Ren<sup>1</sup>, Ya-Xin Zhao<sup>1</sup>, Kenji Watanabe<sup>2</sup>, Takashi Taniguchi<sup>3</sup>, and Lin He<sup>1,\*</sup>

<sup>1</sup>Center for Advanced Quantum Studies, Department of Physics, Beijing Normal University, Beijing 100875, People's Republic of China

<sup>2</sup>Research Center for Functional Materials, National Institute for Materials Science, Tsukuba, Japan

<sup>3</sup>International Center for Materials Nanoarchitectonics, National Institute for Materials Science, Tsukuba, Japan



(Received 29 September 2022; revised 14 January 2023; accepted 1 March 2023; published 15 March 2023)

In twisted bilayer graphene (TBG), a twist-angle-dependent competition between interlayer stacking energy and intralayer elastic energy results in flat rigid layers at large twist angles and lattice reconstruction at small twist angles. Despite enormous scientific interest and effort in the TBG, however, an experimental study of evolution from the rigid lattice to the reconstructed lattice as a function of twist angle is still missing. Here we present a scanning tunneling microscopy and spectroscopy study to reveal the twist-angle-dependent lattice reconstruction in the TBG. Our experiment demonstrates that there is a transition regime between the rigid regime and the relaxed regime, and the reconstructed and unreconstructed structures can coexist in the transition regime. The coexistence of the two distinct structures in this regime may arise from subtle balance between the interlayer stacking energy and intralayer elastic energy in the TBG with intermediate moiré sizes. Our results provide an explanation for inconsistent phase diagrams and tunneling spectra reported in TBG around the magic angle.

DOI: [10.1103/PhysRevB.107.125410](https://doi.org/10.1103/PhysRevB.107.125410)

### I. INTRODUCTION

In two-dimensional van der Waals (vdW) heterojunctions and homojunctions, the competition between the interlayer vdW coupling and the intralayer elastic deformation determines their stacking configurations [1–19], which have profound influences on their electronic and optical properties. For the vdW twist bilayer with a large twist angle (labeled as rigid regime), the size of the moiré pattern is quite small and two flat layers with a rigid lattice are energetically preferable. For the small twist angle case (labeled as relaxed regime), the size of the moiré pattern becomes quite large. Then, to minimize the total energy of the system, there is a strain-accompanied lattice reconstruction that results in large triangular stacking domains and a triangular network of domain walls (DWs) [1–12,20]. The presence of rigid lattice in large twist angle and structural reconstruction in small twist angle have been observed explicitly in a variety of vdW twist bilayers, but, despite enormous scientific interest in the vdW systems, the regime of intermediate twist angles has been the subject of substantially less experimental attention so far. Very recently, Raman measurements on a series of twist MoS<sub>2</sub> bilayers with different twist angles indicate that there is a transition regime between the rigid regime and the relaxed regime [3]. Unlike the rigid and relaxed regimes, the phonon modes of the MoS<sub>2</sub> bilayers evolve rapidly with twist angle in the transition regime [3], suggesting that the structures of the vdW twist bilayers in the transition region are still worth being further studied.

In this work, we reveal the existence of a structural transition regime, in which the reconstructed and unreconstructed structures coexist, in twisted bilayer graphene (TBG). A series of TBG with controlled twist angles  $0.10^\circ < \theta < 3.59^\circ$  are fabricated on hexagonal boron nitride (hBN) and tungsten diselenide (WSe<sub>2</sub>). By using scanning tunneling microscope (STM) and spectroscopy (STS), we directly and systematically study the structures of the TBG. Our experiment demonstrates that there is only rigid lattice for the TBG with  $\theta > 1.80^\circ$  and only reconstructed structure for  $\theta < 0.90^\circ$ , whereas, the reconstructed and unreconstructed structures coexist in the transition regime for  $0.90^\circ < \theta < 1.80^\circ$ .

### II. EXPERIMENT

Figure 1(a) shows schematic of the experimental device setup. The TBG samples are obtained by both dry and wet transfer technology of graphene layer by layer on mechanical-exfoliated hBN and WSe<sub>2</sub> sheets [4,5,21–23] (using the transfer platform from Shanghai Onway Technology Co., Ltd., see Methods of the Supplemental Material for details [24]). Figures 1(b) and 1(c) show schematics of atomic registries in the unreconstructed and reconstructed TBG, respectively. For the unreconstructed TBG, the stacking structure is formed by introducing a twist between two rigid graphene layers. For the reconstructed TBG, to reduce the total energy of the system, the AB and BA stacking regions are enlarged with separating narrow DWs and, simultaneously, the AA stacking regions are reduced. Therefore, we can distinguish the unreconstructed and reconstructed TBG in two different ways in the STM measurements. The first method is based on the emergence of the DWs in the reconstructed TBG.

\*Correspondence and requests for materials should be addressed to: [helin@bnu.edu.cn](mailto:helin@bnu.edu.cn)

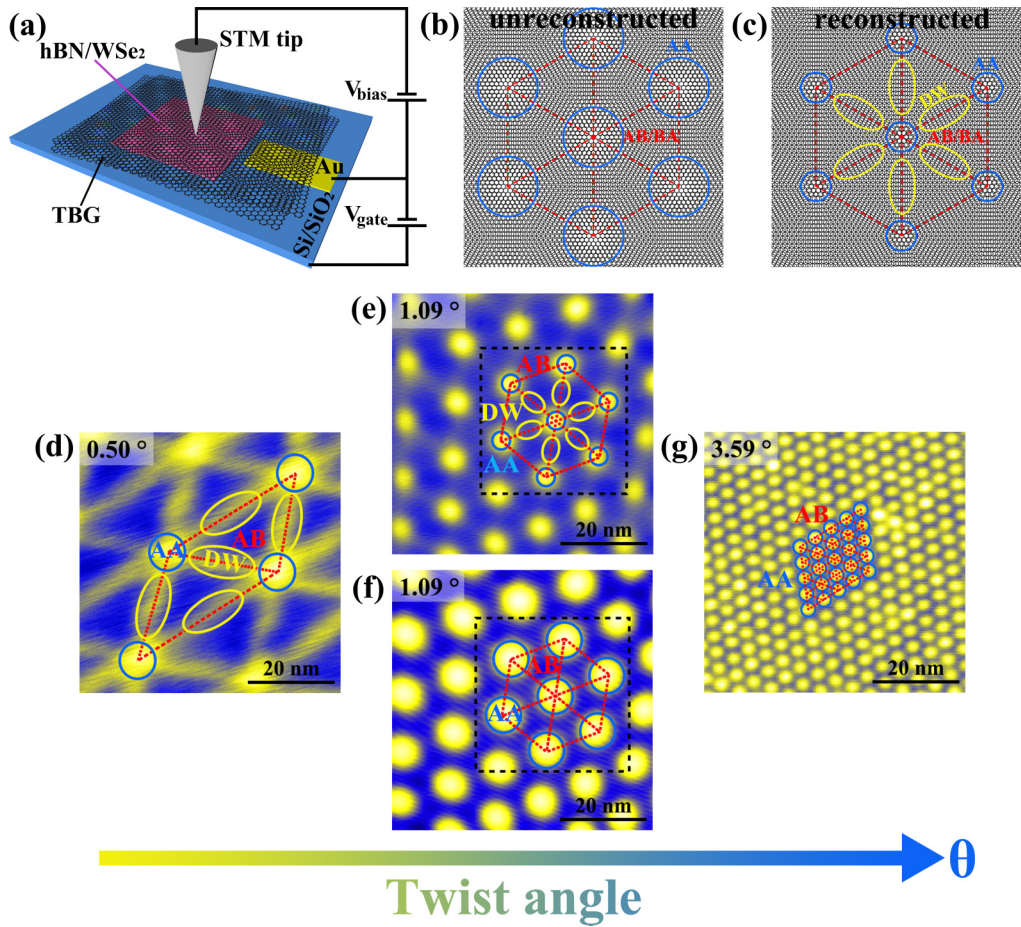


FIG. 1. (a) Schematic of the experimental device setup. (b) and (c) Schematic of atomic registries in unreconstructed and reconstructed TBG, respectively. The blue and yellow circles represent the AA and DW regions, respectively. The rest of the red triangles are the AB/BA regions. (d)–(g) Representative STM images of the obtained TBG with different twist angles. The scanning parameters are  $V_{\text{bias}} = 0.6$  V,  $I = 100$  pA (d),  $V_{\text{bias}} = 0.5$  V,  $I = 100$  pA (e),  $V_{\text{bias}} = 0.3$  V,  $I = 100$  pA (f),  $V_{\text{bias}} = 0.8$  V,  $I = 200$  pA (g).

The second method is based on the relative size of the AA and the AB (BA) stacking regions. Figures 1(d)–1(g) show several representative STM images of the obtained TBG with different twist angles in our experiment (see more STM images in Figs. S2 and S3 [24]). The moiré superlattice can be clearly identified from the periodic corrugations in the images and the twist angles can be obtained based on the measured periods  $D$  according to  $D = a/[2\sin(\theta/2)]$ , where  $a \approx 0.246$  nm. The twist angle  $\theta$  can also be roughly measured according to the fast Fourier transforms (FFT) of the STM images and the results of both methods are consistent (see Fig. S4 for details). In the  $0.50^\circ$  TBG, the area of the AA regions is much smaller than that of the AB/BA regions and there are one-dimensional (1D) DWs between two adjacent AB and BA regions [Fig. 1(d)], as observed previously in the reconstructed TBG [2, 4–6, 10–12]. In contrast, the structures of the  $3.59^\circ$  TBG can be interpreted based on a rigid lattice picture [Fig. 1(g)]. Such a result is consistent with previous understanding. However, in our experiment, it is quite surprising to observe two distinct structures of the  $1.09^\circ$  TBG: one is in the rigid structure [Fig. 1(f)], the other is in the relaxed structure [Fig. 1(e)]. This result indicates that the structure in the TBG with the intermediate twist angles (labeled as transition regime) is quite different from that of the rigid regime and the relaxed regime

(see Figs. S5–S7 for coexistence of unreconstructed and reconstructed TBG structures in the single topographic map [24]).

### III. RESULTS AND DISCUSSION

The distinct features of the two structures of the  $1.09^\circ$  TBG can be seen more clearly in the zoom-in STM images, as shown in Figs. 2(a) and 2(c). To quantitatively show the differences between the two structures, Figs. 2(b) and 2(d) show height profiles along dashed lines in Figs. 2(a) and 2(c), respectively, which reflect the topographic changes that pass through different regions of the TBG successively. In the reconstructed TBG, a well-defined corrugated DW can be detected, whereas it becomes almost undetectable in the unreconstructed TBG. To systematically study the twist-angle-dependent structures, we measure averaged  $H_{\text{DW}}/H_{\text{AA}}$  as a function of the twist angles for more than 60 TBGs (here,  $H_{\text{DW}}$  and  $H_{\text{AA}}$  are the height of the DW and AA regions measured according to the height profiles), as summarized in Fig. 2(e). The error bars reflect the height fluctuations measured on different AA and DW regions and we should point out that the obtained result in this work is independent of the substrates. It is easy to find that the measured results can be

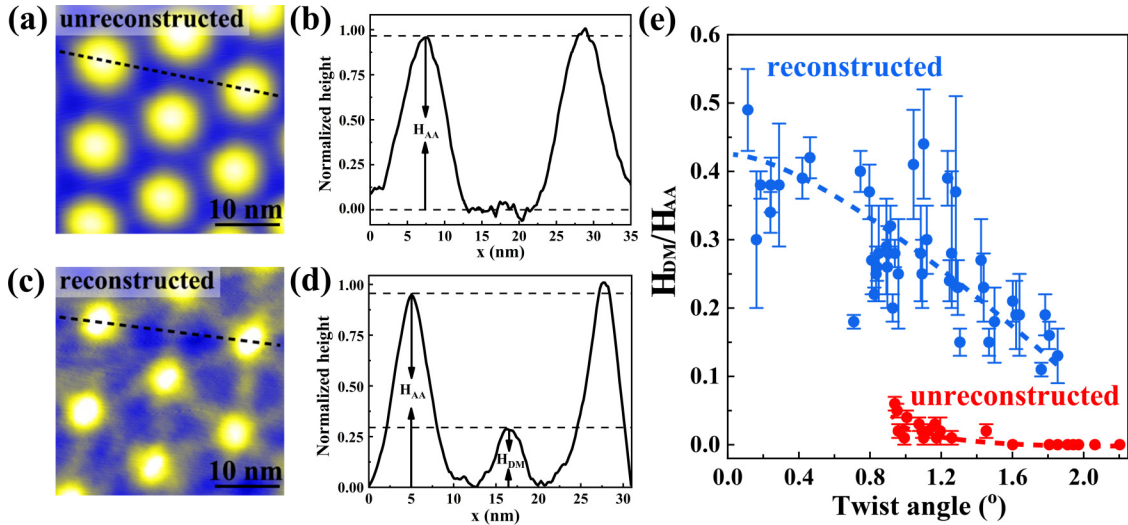


FIG. 2. (a) and (c) Zoom-in STM images of the TBGs in Figs. 1(f) and 1(e), respectively. (b) and (d) Height profiles along dashed lines in (a) and (c), respectively. The height of AA and DW regions are marked in the figures. (e) The measured  $H_{DW}/H_{AA}$  as a function of the twist angles for different TBG devices. The red and blue points represent the results obtained in the unreconstructed and reconstructed TBG devices, respectively. The error bars reflect the standard error of the data.

divided into two categories: the large (small) values of the ratio  $H_{DW}/H_{AA}$  indicate that the TBG has a relaxed (rigid) lattice. According to the result in Fig. 2(e), there is only reconstructed structure for the TBG with  $\theta < 0.90^\circ$  and only rigid lattice for  $\theta > 1.80^\circ$ . The onset of reconstruction begins below about  $1.80^\circ$ , which is in good agreement with that reported in previous studies [10,20]. Besides that, there is a transition regime,  $0.90^\circ < \theta < 1.80^\circ$ , in which both the reconstructed and unreconstructed structures coexist. Here we should point out that both the reconstructed and unreconstructed structures are quite stable during our STM measurements. The two distinct structures will result in quite different electronic properties of the TBG in the transition regime, which may provide a consistent understanding of different STS spectra and phase diagrams observed previously in magic-angle TBG (the magic angle  $\sim 1.08^\circ$  is in the transition regime) [29–34]. In some magic-angle TBG, the superconducting phase is observed around the insulating phase. Whereas, in the other magic-angle TBG, there is no correlation-induced insulating phase along with the superconducting phase [33]. Our results provide an explanation for the inconsistent phase diagrams that may arise from the reconstructed and unreconstructed structures, respectively.

Besides the DWs, we also can distinguish the reconstructed and unreconstructed structures of the TBG according to the relative size of the AA and the AB (BA) stacking regions. However, it is quite difficult to exactly define the AA stacking region based on the height profiles of the STM images [see Figs. 2(b) and 2(d) as examples]. To overcome this challenge, we carry out measurement of spatial distribution of the low-energy van Hove singularities (VHSs) to measure the area of the AA stacking region. In the TBG, a finite interlayer coupling the two adjacent layers generates a pair of saddle points, which introduce two pronounced VHSs in density of states (DOS) [35–41]. The two low-energy VHSs are mainly localized in the AA stacking region, especially for the TBG

with twist angles  $\theta < 2.0^\circ$  [29,37–39]. Figure 3(a) shows representative STS spectra measured along the dashed line in Fig. 2(c) (here the back-gate voltage is 14 V. See STS spectroscopic map as a function of  $V_{\text{gate}}$ , Fig. S8, taken in different TBG [24]). The two pronounced peaks in the spectra recorded in the AA stacking regions are attributed to the two low-energy VHSs of the TBG. Figure 3(b) shows a typical STS map recorded at the energy of one of the VHS, which directly reflects the spatial distribution of the DOS. Obviously, the electronic states of the VHS are mainly localized in the AA region of the TBG. Figure 3(c) displays a profile line of the DOS at the energy of the VHS along the dashed line in Fig. 3(b), which is used to estimate the size of the AA stacking region. To quantitatively describe the size of the AA stacking region, a Gaussian curve fitting is used to obtain the standard deviation  $\sigma$  of the profile line [42–46], as shown in Fig. 3(c) (see Supplemental Material for details of analysis [24]). For each TBG, the  $\sigma$  is averaged by fitting the DOS along the three moiré directions. Figure 3(d) summarizes the averaged  $\sigma$  as a function of twist angles based on part of the TBG devices in Fig. 2(e). Obviously, the twist-angle-dependent sizes of the AA stacking regions for the reconstructed and unreconstructed TBG are quite different (the two structures of the TBG are categorized based on the results of Fig. 2). As expected, the sizes of the AA stacking regions in the unreconstructed TBGs increase quickly with the decrease of twist angle, whereas, they depend weakly on the twist angle in the reconstructed TBGs. Such a result is quite reasonable because the area of the AA stacking regions in the reconstructed TBG should be significantly reduced to lower down the stacking energy of the system. Here we should point out that the boundaries of the three regimes in the TBG are determined according to the result of Fig. 2 in our experiment. For the method shown in Fig. 3, we can distinguish the reconstructed and unreconstructed structures for  $\theta < 1.4^\circ$ . However, it is impossible to distinguish the reconstructed and unreconstructed structures for  $\theta > 1.4^\circ$ .

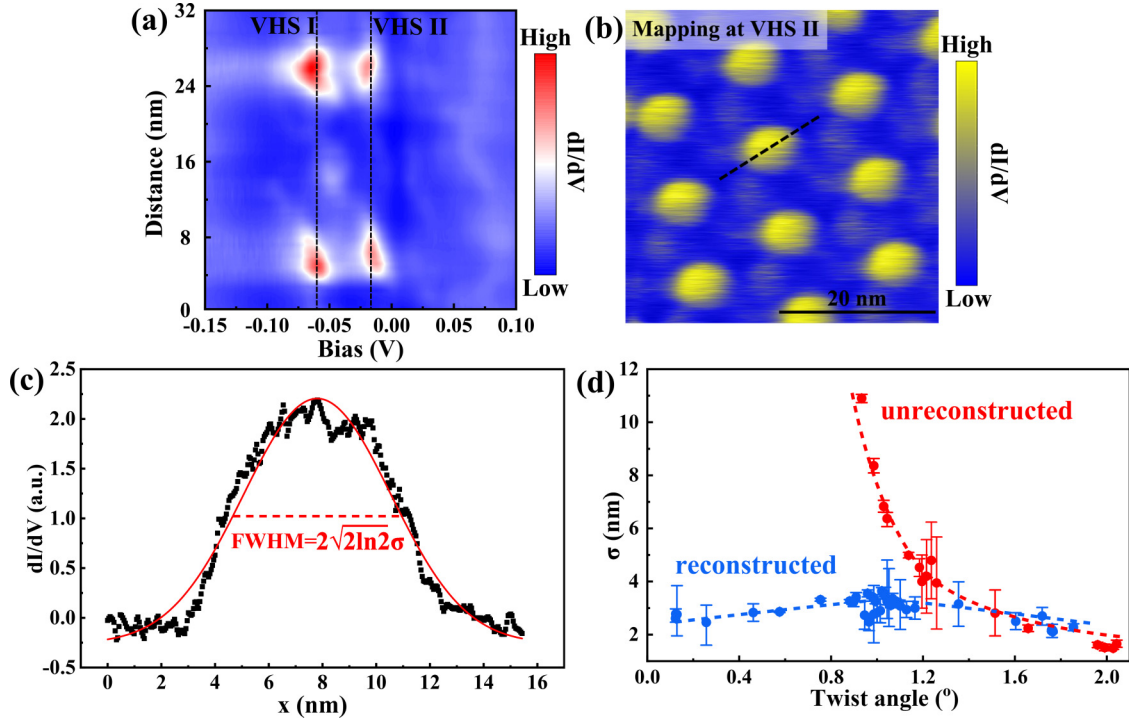


FIG. 3. (a) Representative STS spectra measured along the dashed line in Fig. 2(c). Two low-energy VHSs are observed in the AA regions. (b) A typical STS map recorded at the energy of VHS II ( $V_{\text{bias}} = -0.018$  V,  $I = 40$  pA,  $V_{\text{gate}} = 14$  V). (c) A profile line of the DOS along the dashed line in (b). The red solid curve represents a Gaussian fitting of the DOS distribution, and the red dashed line represents the full width at half-maximum (FWHM) of the Gaussian fitting. (d) The averaged  $\sigma$  as a function of twist angles based on results obtained from part of the TBG devices in Fig. 2(e). The red and blue points represent results of the unreconstructed and reconstructed TBG devices, respectively. The error bars reflect the standard error of the data.

To further understand the observed phenomena, we calculate the stacking energies of both the reconstructed and unreconstructed TBG as a function of twist angles, according to the theoretical results in Refs. [10,47]. In the calculation, the total atoms of different TBGs are assumed to be the same and are equal to the number of atoms in a moiré unit cell of the calculated TBG with the minimum twist angle, as schematically shown in inset of Fig. 4(a). For the reconstructed TBG, the

areas for the AA, AB, and DW regions in different twist angles are extracted from the results obtained in Ref. [10] (see Supplemental Material for details of calculation [24]). For the unreconstructed TBG, two different interlayer distances are considered in the calculation and the real interlayer distance  $d$  of the TBG is expected to be within them, i.e.,  $3.2 \text{ \AA} \leq d \leq 3.6 \text{ \AA}$  [48]. Figure 4(a) shows the calculated vdW stacking energies as a function of twist angles for both

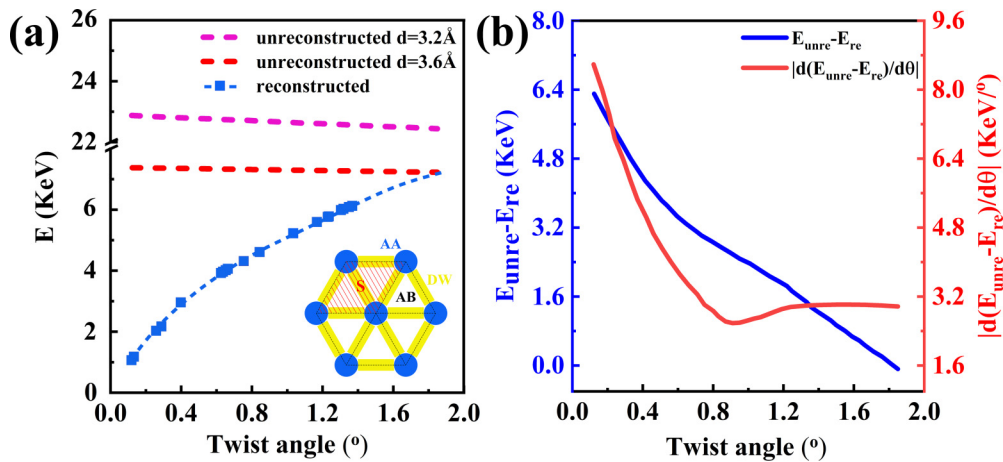


FIG. 4. (a) The calculated vdW stacking energy as a function of twist angles for both the reconstructed and unreconstructed TBG. The red and pink dashed curves are calculated with different interlayer distances. The inset shows schematic of stacking order assignments. The red shade part represents the area of the moiré unit cell. (b) The difference of vdW stacking energy between the unreconstructed and reconstructed TBG (blue curve) and the absolute value of deviation of the vdW energy difference (red curve) as a function of twist angles.

the reconstructed and unreconstructed TBG. The energy difference between them is shown in Fig. 4(b) (here we use the result of  $d = 3.6 \text{ \AA}$  for the unreconstructed TBG for simplicity and the result of other distances is similar). For very small twist angles, the vdW stacking energy of the reconstructed TBGs is much smaller than that of the unreconstructed TBGs. Then, the TBG prefers to expand the  $AB$  and  $BA$  regions to gain vdW energy, which is much larger than the losing elastic energy in the formation of the DWs. Therefore, we always observe the reconstructed structures for the TBG with very small twist angles. With increasing the twist angle, the energy of the unreconstructed TBGs decreases slowly, while the energy of the reconstructed TBGs increases quickly. At a sufficiently large twist angle, the gaining vdW stacking energy cannot compensate for the losing elastic energy in the TBG. Then, the TBG prefers to be in the structure consisting of two rigid layers. As a consequence, we always observe the unreconstructed structures for the TBG with large twist angles. For the TBG with intermediate twist angles between that of the rigid regime and the relaxed regime, the difference of the vdW energies between the two structures is not quite large. Then, the subtle balance between the gaining vdW energy and the losing elastic energy makes both the reconstructed and unreconstructed TBG energetically stable. Consequently, we observe both the structures in the transition region in our experiment. In Fig. 4(b), the derivative of the vdW energy difference between the reconstructed and unreconstructed TBGs

as a function of the twist angle is also plotted. It is interesting to find that the absolute value of the derivation increases rapidly below a critical twist angle,  $\sim 0.9^\circ$ , which means that the energy difference between the reconstructed and unreconstructed TBG increases much quicker below the critical twist angle. Such a result helps us to further understand the experimental result that there is only reconstructed TBG for  $\theta < 0.90^\circ$ .

#### IV. CONCLUSIONS

In summary, we systematically study structures of the TBGs and demonstrate that there are three regimes categorized by their structures. In the transition regime,  $0.90^\circ < \theta < 1.80^\circ$ , both the reconstructed and unreconstructed structures coexist in the studied TBG. Our analysis indicates that subtle balance between the interlayer stacking energy and intralayer elastic energy in the TBG with intermediate moiré sizes leads to the coexistence of the two structures in the transition regime.

#### ACKNOWLEDGMENT

This work was supported by the National Key R and D Program of China (Grants No. 2021YFA1400100 and No. 2021YFA1401900) and National Natural Science Foundation of China (Grants No. 12141401 and No. 11974050).

- 
- [1] C. R. Woods, L. Britnell, A. Eckmann, R. S. Ma, J. C. Lu, H. M. Guo, X. Lin, G. L. Yu, Y. Cao, R. V. Gorbachev *et al.*, Commensurate–incommensurate transition in graphene on hexagonal boron nitride, *Nat. Phys.* **10**, 451 (2014).
  - [2] H. Yoo, R. Engelke, S. Carr, S. Fang, K. Zhang, P. Cazeaux, S. H. Sung, R. Hovden, A. W. Tsen, T. Taniguchi *et al.*, Atomic and electronic reconstruction at the van Der Waals interface in twisted bilayer graphene, *Nat. Mater.* **18**, 448 (2019).
  - [3] J. Quan, L. Linhart, M.-L. Lin, D. Lee, J. Zhu, C.-Y. Wang, W.-T. Hsu, J. Choi, J. Embley, C. Young *et al.*, Phonon renormalization in reconstructed MoS<sub>2</sub> moiré superlattices, *Nat. Mater.* **20**, 1100 (2021).
  - [4] Y.-W. Liu, Y. Su, X.-F. Zhou, L.-J. Yin, C. Yan, S.-Y. Li, W. Yan, S. Han, Z.-Q. Fu, Y. Zhang *et al.*, Tunable Lattice Reconstruction, Triangular Network of Chiral One-Dimensional States, and Bandwidth of Flat Bands in Magic Angle Twisted Bilayer Graphene, *Phys. Rev. Lett.* **125**, 236102 (2020).
  - [5] Q. Zheng, C.-Y. Hao, X.-F. Zhou, Y.-X. Zhao, J.-Q. He, and L. He, Tunable Sample-Wide Electronic Kagome Lattice in Low-Angle Twisted Bilayer Graphene, *Phys. Rev. Lett.* **129**, 076803 (2022).
  - [6] A. C. Gadelha, D. A. Ohlberg, C. Rabelo, E. G. Neto, T. L. Vasconcelos, J. L. Campos, J. S. Lemos, V. Ornelas, D. Miranda, R. Nadas *et al.*, Localization of lattice dynamics in low-angle twisted bilayer graphene, *Nature (London)* **590**, 405 (2021).
  - [7] A. Weston, Y. Zou, V. Enaldiev, A. Summerfield, N. Clark, V. Zólyomi, A. Graham, C. Yelgel, S. Magorrian, M. Zhou *et al.*, Atomic reconstruction in twisted bilayers of transition metal dichalcogenides, *Nat. Nanotech.* **15**, 592 (2020).
  - [8] E. Li, J.-X. Hu, X. Feng, Z. Zhou, L. An, K. T. Law, N. Wang, and N. Lin, Lattice reconstruction induced multiple ultra-flat bands in twisted bilayer WSe<sub>2</sub>, *Nat. Commun.* **12**, 5601 (2021).
  - [9] D. Huang, J. Choi, C.-K. Shih, and X. Li, Excitons in semiconductor moiré superlattices, *Nat. Nanotech.* **17**, 227 (2022).
  - [10] N. P. Kazmierczak, M. Van Winkle, C. Ophus, K. C. Bustillo, S. Carr, H. G. Brown, J. Ciston, T. Taniguchi, K. Watanabe, and D. K. Bediako, Strain fields in twisted bilayer graphene, *Nat. Mater.* **20**, 956 (2021).
  - [11] L. J. McGilly, A. Kerelsky, N. R. Finney, K. Shapovalov, E.-M. Shih, A. Ghiotto, Y. Zeng, S. L. Moore, W. Wu, Y. Bai *et al.*, Visualization of moiré superlattices, *Nat. Nanotech.* **15**, 580 (2020).
  - [12] J.-B. Qiao, L.-J. Yin, and L. He, Twisted graphene bilayer around the first magic angle engineered by heterostrain, *Phys. Rev. B* **98**, 235402 (2018).
  - [13] S. Carr, S. Fang, Z. Zhu, and E. Kaxiras, Exact continuum model for low-energy electronic states of twisted bilayer graphene, *Phys. Rev. Res.* **1**, 013001 (2019).
  - [14] N. N. T. Nam and M. Koshino, Lattice relaxation and energy band modulation in twisted bilayer graphene, *Phys. Rev. B* **96**, 075311 (2017).
  - [15] S. Carr, D. Massatt, S. B. Torrisi, P. Cazeaux, M. Luskin, and E. Kaxiras, Relaxation and domain formation in incommensurate two-dimensional heterostructures, *Phys. Rev. B* **98**, 224102 (2018).
  - [16] M. M. van Wijk, A. Schuring, M. I. Katsnelson, and A. Fasolino, Relaxation of moiré patterns for slightly misaligned identical lattices: Graphene on graphite, *2D Mater.* **2**, 034010 (2015).

- [17] K. Zhang and E. B. Tadmor, Structural and electron diffraction scaling of twisted graphene bilayers, *J. Mech. Phys. Solids* **112**, 225 (2018).
- [18] F. Gargiulo and O. V. Yazyev, Structural and electronic transformation in low-angle twisted bilayer graphene, *2D Mater.* **5**, 015019 (2017).
- [19] N. R. Walet and F. Guinea, The emergence of one-dimensional channels in marginal-angle twisted bilayer graphene, *2D Mater.* **7**, 015023 (2019).
- [20] Y.-N. Ren, Z. Zhan, Y.-W. Liu, C. Yan, S. Yuan, and L. He, Real-space mapping of local sub-degree lattice rotations in twisted bilayer graphene magnified by moiré superlattices, *Nano Lett.* **23**, 1836 (2023).
- [21] C. Yan, D.-L. Ma, J.-B. Qiao, H.-Y. Zhong, L. Yang, S.-Y. Li, Z.-Q. Fu, Y. Zhang, and L. He, Scanning tunneling microscopy study of the quasicrystalline 30° twisted bilayer graphene, *2D Mater.* **6**, 045041 (2019).
- [22] Y. Zhang, Z. Hou, Y.-X. Zhao, Z.-H. Guo, Y.-W. Liu, S.-Y. Li, Y.-N. Ren, Q.-F. Sun, and L. He, Correlation-induced valley splitting and orbital magnetism in a strain-induced zero-energy flatband in twisted bilayer graphene near the magic angle, *Phys. Rev. B* **102**, 081403(R) (2020).
- [23] S. Jin, M. Huang, Y. Kwon, L. Zhang, B.-W. Li, S. Oh, J. Dong, D. Luo, M. Biswal, B. V. Cunniff *et al.*, Colossal grain growth yields single-crystal metal foils by contact-free annealing, *Science* **362**, 1021 (2018).
- [24] See Supplemental Material at <http://link.aps.org/supplemental/10.1103/PhysRevB.107.125410> for more experimental data, analysis and details of discussion, which includes Refs. [25–28].
- [25] Z. Zhang, X. Xu, Z. Zhang, M. Wu, J. Wang, C. Liu, N. Shang, J. Wang, P. Gao, D. Yu *et al.*, Identification of copper surface index by optical contrast, *Adv. Mater. Interf.* **5**, 1800377 (2018).
- [26] K. Kim, S. Coh, L. Z. Tan, W. Regan, J. M. Yuk, E. Chatterjee, M. F. Crommie, M. L. Cohen, S. G. Louie, and A. Zettl, Raman Spectroscopy Study of Rotated Double-Layer Graphene: Misorientation-Angle Dependence of Electronic Structure, *Phys. Rev. Lett.* **108**, 246103 (2012).
- [27] C. R. Dean, A. F. Young, I. Meric, C. Lee, L. Wang, S. Sorgenfrei, K. Watanabe, T. Taniguchi, P. Kim, K. L. Shepard *et al.*, Boron nitride substrates for high-quality graphene electronics, *Nat. Nanotech.* **5**, 722 (2010).
- [28] X.-F. Zhou, Y.-W. Liu, H.-Y. Yan, Z.-Q. Fu, H. Liu, and L. He, Electronic confinement in quantum dots of twisted bilayer graphene, *Phys. Rev. B* **104**, 235417 (2021).
- [29] L.-J. Yin, J.-B. Qiao, W.-J. Zuo, W.-T. Li, and L. He, Experimental evidence for non-Abelian gauge potentials in twisted graphene bilayers, *Phys. Rev. B* **92**, 081406(R) (2015).
- [30] Y. Xie, B. Lian, B. Jäck, X. Liu, C.-L. Chiu, K. Watanabe, T. Taniguchi, B. A. Bernevig, and A. Yazdani, Spectroscopic signatures of many-body correlations in magic-angle twisted bilayer graphene, *Nature (London)* **572**, 101 (2019).
- [31] A. Kerelsky, L. J. McGilly, D. M. Kennes, L. Xian, M. Yankowitz, S. Chen, K. Watanabe, T. Taniguchi, J. Hone, C. Dean *et al.*, Maximized electron interactions at the magic angle in twisted bilayer graphene, *Nature (London)* **572**, 95 (2019).
- [32] Y. Jiang, X. Lai, K. Watanabe, T. Taniguchi, K. Haule, J. Mao, and E. Y. Andrei, Charge order and broken rotational symmetry in magic-angle twisted bilayer graphene, *Nature (London)* **573**, 91 (2019).
- [33] Y. Choi, J. Kemmer, Y. Peng, A. Thomson, H. Arora, R. Polski, Y. Zhang, H. Ren, J. Alicea, G. Refael *et al.*, Electronic correlations in twisted bilayer graphene near the magic angle, *Nat. Phys.* **15**, 1174 (2019).
- [34] L. Balents, C. R. Dean, D. K. Efetov, and A. F. Young, Superconductivity and strong correlations in moiré flat bands, *Nat. Phys.* **16**, 725 (2020).
- [35] R. Bistritzer and A. H. MacDonald, Moiré bands in twisted double-layer graphene, *Proc. Natl Acad. Sci. USA* **108**, 12233 (2011).
- [36] J. M. B. Lopes dos Santos, N. M. R. Peres, and A. H. Castro Neto, Graphene Bilayer with a Twist: Electronic Structure, *Phys. Rev. Lett.* **99**, 256802 (2007).
- [37] G. Li, A. Luican, J. M. B. Lopes dos Santos, A. H. Castro Neto, A. Reina, J. Kong, and E. Y. Andrei, Observation of van Hove singularities in twisted graphene layers, *Nat. Phys.* **6**, 109 (2010).
- [38] W. Yan, M. Liu, R.-F. Dou, L. Meng, L. Feng, Z.-D. Chu, Y. Zhang, Z. Liu, J.-C. Nie, and L. He, Angle-Dependent Van Hove Singularities in a Slightly Twisted Graphene Bilayer, *Phys. Rev. Lett.* **109**, 126801 (2012).
- [39] A. Luican, G. Li, A. Reina, J. Kong, R. R. Nair, K. S. Novoselov, A. K. Geim, and E. Y. Andrei, Single-Layer Behavior and Its Breakdown in Twisted Graphene Layers, *Phys. Rev. Lett.* **106**, 126802 (2011).
- [40] I. Brihuega, P. Mallet, H. González-Herrero, G. T. De Laissardière, M. M. Ugeda, L. Magaud, J. M. Gómez-Rodríguez, F. Ynduráin, and J.-Y. Veuille, Unraveling the Intrinsic and Robust Nature of Van Hove Singularities in Twisted Bilayer Graphene by Scanning Tunneling Microscopy and Theoretical Analysis, *Phys. Rev. Lett.* **109**, 196802 (2012).
- [41] T. Ohta, J. T. Robinson, P. J. Feibelman, A. Bostwick, E. Rotenberg, and T. E. Beechem, Evidence for Interlayer Coupling and Moiré Periodic Potentials in Twisted Bilayer Graphene, *Phys. Rev. Lett.* **109**, 186807 (2012).
- [42] C. Lee, X. Wei, J. W. Kysar, and J. Hone, Measurement of the Elastic Properties and Intrinsic Strength of Monolayer Graphene, *Science* **321**, 385 (2008).
- [43] A. Shekhawat and R. O. Ritchie, Toughness and strength of nanocrystalline graphene, *Nat. Commun.* **7**, 10546 (2016).
- [44] J. C. Meyer, A. K. Geim, M. I. Katsnelson, K. S. Novoselov, T. J. Booth, and S. Roth, The structure of suspended graphene sheets, *Nature (London)* **446**, 60 (2007).
- [45] J. Xue, J. Sanchez-Yamagishi, D. Bulmash, P. Jacquod, A. Deshpande, K. Watanabe, T. Taniguchi, P. Jarillo-Herrero, and B. J. LeRoy, Scanning tunnelling microscopy and spectroscopy of ultra-flat graphene on hexagonal boron nitride, *Nat. Mater.* **10**, 282 (2011).
- [46] L. A. Ponomarenko, R. Yang, R. V. Gorbachev, P. Blake, A. S. Mayorov, K. S. Novoselov, M. I. Katsnelson, and A. K. Geim, Density of States and Zero Landau Level Probed through Capacitance of Graphene, *Phys. Rev. Lett.* **105**, 136801 (2010).
- [47] F. Peymanirad, S. K. Singh, H. Ghorbanfekr-Kalashami, K. S. Novoselov, F. M. Peeters, and M. Neek-Amal, Thermal Activated Rotation of Graphene Flake on Graphene, *2D Mater.* **4**, 025015 (2017).
- [48] Y.-X. Zhao, X.-F. Zhou, Y. Zhang, and L. He, Oscillations of the Spacing Between Van Hove Singularities Induced by Sub-Angstrom Fluctuations of Interlayer Spacing in Graphene Superlattices, *Phys. Rev. Lett.* **127**, 266801 (2021).